



Research Repository UCD

Title	Dynamic axle force and road profile identification using a moving vehicle
Authors(s)	McGetrick, P., Kim, Chul-Woo, González, Arturo, et al.
Publication date	2013
Publication information	McGetrick, P., Chul-Woo Kim, Arturo González, and et al. "Dynamic Axle Force and Road Profile Identification Using a Moving Vehicle." International Association for Sustainable Development and Management, 2013.
Publisher	International Association for Sustainable Development and Management
Item record/more information	http://hdl.handle.net/10197/4879

Downloaded 2025-12-04 23:02:38

The UCD community has made this article openly available. Please share how this access benefits you. Your story matters! (@ucd_oa)



© Some rights reserved. For more information

Dynamic axle force and road profile identification using a moving vehicle

Patrick J. McGetrick^{*1}, Chul-Woo Kim², Arturo González³, Eugene J. OBrien⁴

^{*1,2} *Dept. of Civil and Earth Resources Engineering, Kyoto University, Kyoto 615-8540, Japan*

^{*1} mcgetrick.patrickjohn.5x@kyoto-u.ac.jp, ² kim.chulwoo.5u@kyoto-u.ac.jp

^{3,4} *School of Civil, Structural and Environmental Engineering, University College Dublin, Belfield, Dublin 4, Ireland*

³ arturo.gonzalez@ucd.ie, ⁴ eugene.obrien@ucd.ie

ABSTRACT

In the interaction between vehicles, pavements and bridges, it is essential to aim towards a reduction of vehicle axle forces to promote longer pavement life spans and to prevent bridges loads becoming too high. Moreover, as the road surface roughness affects the vehicle dynamic forces, an efficient monitoring of pavement condition is also necessary to achieve this aim. This paper uses a novel algorithm to identify the dynamic interaction forces and pavement roughness from vehicle accelerations in both theoretical simulations and a laboratory experiment; moving force identification theory is applied to a vehicle model for this purpose. Theoretical simulations are employed to evaluate the ability of the algorithm to predict forces over a range of bridge spans and to evaluate the influence of road roughness level on the accuracy of the results. Finally, in addressing the challenge for the real-world problem, the effects of vehicle configuration and speed on the predicted road roughness are also investigated in a laboratory experiment.

Keywords: Acceleration, dynamic axle forces, inverse dynamics, laboratory experiment, pavement roughness, vehicle-bridge interaction.

1. INTRODUCTION

Dynamic vehicle axle forces can increase the average road surface damage by up to four times compared to that caused by static axle forces alone (Cebon 1987; Cole and Cebon 1992). Therefore, minimising these dynamic axle forces has obvious benefits relating to life span extension and reduction of the loading on pavement and bridges. Furthermore, as the road surface roughness also influences these dynamic forces, it is essential that road profiles for highways and bridges are monitored and maintained (Kitching et al. 2000).

There are several existing methods for vehicle axle force identification. These include methods which use direct instrumentation and measurements of vehicle axles to obtain the force history; some examples are wheel hub transducers, air spring pressure transducer systems and laser detectors. A comprehensive review of these and other direct methods is provided by Davis and Bunker (2007). The accuracy of these methods can be quite good but

they are also costly and in some cases difficult to install. As the dynamic axle forces are of particular importance for short to medium span bridges, a considerable amount of research has been undertaken which focuses on methods utilising the moving force identification (MFI) technique. This technique is based on well-established general inverse problem theory and identifies the vehicle-bridge interaction forces indirectly via measurements on the bridge. Yu and Chan (2007) provide a comprehensive literature review of this research, which ranges from methods using exact solutions and forms of system identification (Law et al. 1997) to those that incorporate Tikhonov regularisation (Law et al. 2001). In recent years, methods based on finite element (FE) models have been proposed (Law et al. 2004; Deng and Cai 2010b). However, these approaches also have some drawbacks which can limit their practical implementation; they can be time consuming and costly due to the necessity to install data acquisition equipment on site and obtain measurements at a number of locations on the bridge.

A number of methods exist for the measurement of road profiles, including both static manual methods and dynamic approaches (Sayers and Karamihas 1996, 1998). Dynamic approaches, such as inertial profilometers, can be quite efficient and highly accurate as they can measure profile tracks at highway speeds and incorporate laser height sensing devices in a vehicle. Accelerometers are used to remove the effects of vehicle dynamics from the elevation measurements. However, due to the laser-based technology, this type of approach can be quite expensive. More recently, low cost approaches have been proposed which address this issue by utilising vehicle accelerations only in order to characterise or identify road profile heights (González et al. 2008a; Harris et al. 2010). The approach numerically validated by Harris et al. (2010) is based on a combinatorial optimisation algorithm and can identify road profile heights very accurately. It takes a computational time of approximately 5 hours to identify the road profile heights in parallel wheel tracks in a 100m long profile.

In this paper, the results of a novel algorithm for the identification of both dynamic vehicle forces and pavement profile heights are presented from both theoretical simulations and a laboratory experiment. The low-cost approach presented here has the benefit of only requiring direct instrumentation of the vehicle with accelerometers; all data acquisition electronics and measuring equipment are contained within the vehicle thus no bridge installations are required. In order to identify the dynamic forces between the vehicle and the road and/or bridge from the vehicle accelerations, MFI theory is applied to the vehicle equations of motion. An advantage of this approach is that its methodology allows for the prediction of the road pavement roughness experienced by the vehicle and in this regard, it improves upon the computational time required by the algorithm proposed by Harris et al. (2010). Furthermore, the ability to identify the road roughness profile experienced by a vehicle as it crosses a bridge would have many benefits in the field of vehicle-bridge interaction (VBI) assessment as it is an important component of the VBI. A numerical validation of the novel algorithm implemented in this paper was carried out first by OBrien et al. (2012). Therefore, this paper aims to validate this algorithm for a wider range of simulated scenarios in addition to investigating its implementation in a laboratory experiment. For this purpose, a coupled VBI model is used to simulate ‘measured’ accelerations for a vehicle travelling over bridge spans of 15, 25 and 35 metres, road profiles ranging from ISO class A

(very good) to E (very poor) (ISO 8608 1995) and at a speed of 80 km/h (22 m/s). Measurements from a laboratory experiment are analysed for two vehicle configurations and three vehicle speeds.

2. METHODOLOGY

2.1 Theoretical Scenarios

The coupled VBI model used in theoretical simulations consists of a 4 degree-of-freedom half-car vehicle model crossing over a simply supported finite element (FE) beam at constant speed, c (Figure 1) and it is described in detail by OBrien et al. (2012). Examples of other coupled and uncoupled VBI models can be found in a review by González (2010). A sampling frequency of 1000 Hz is used in all simulations. Only the details of the model required for elaboration of the force identification algorithm are presented here.

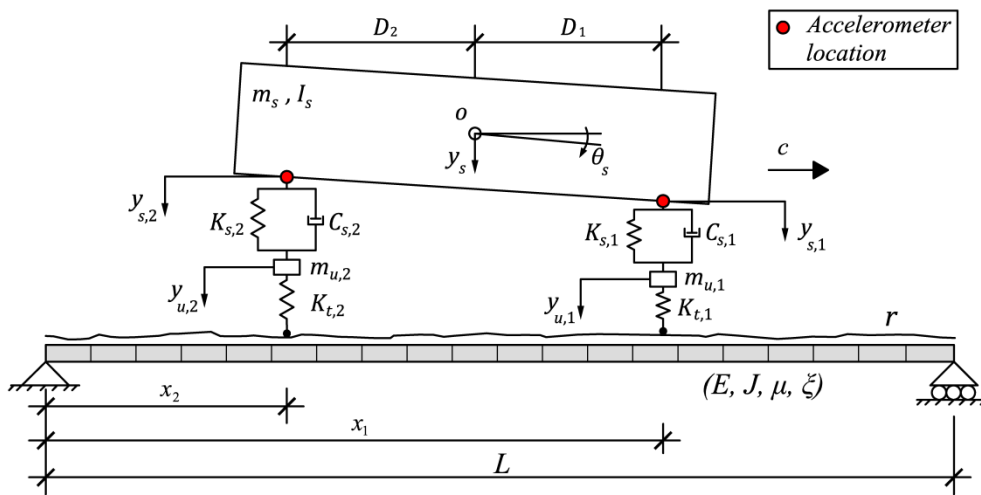


Figure 1. Vehicle-bridge interaction model

2.1.1 Vehicle model

The properties of the half-car model are listed in Table 1. Its geometry is based on manufacturer specifications for a two axle truck (DAF 2011) and typical mechanical properties have been gathered from existing literature (Cebon 1999; Harris et al. 2007; González et al. 2010). The equations of motion of the vehicle are obtained by imposing equilibrium of all forces and moments acting on the vehicle and expressing them in terms of the degrees of freedom. For the purposes of the algorithm formulation used throughout this paper, the vehicle equations of motion are represented by Eq. (1):

$$\mathbf{M}_v \ddot{\mathbf{y}}_v + \mathbf{C}_v \dot{\mathbf{y}}_v + \mathbf{K}_v \mathbf{y}_v = \mathbf{f}_v \quad (1)$$

where \mathbf{M}_v , \mathbf{C}_v , and \mathbf{K}_v are, respectively, the mass, damping and stiffness matrices of the vehicle. The displacement vector of the vehicle is $\mathbf{y}_v = \{y_s, \theta_s, y_{u,1}, y_{u,2}\}^T$, while the vector,

\mathbf{f}_v , contains the time varying interaction forces applied by the vehicle to the road and/or bridge.

$$\mathbf{f}_v = \{0 \quad 0 \quad -F_{t,1} \quad -F_{t,2}\}^T \quad (2)$$

Table 1 Properties of vehicle model

Property	Unit	Symbol	Value
Body mass	kg	m_s	16 200
Axle mass	kg	$m_{u,1}$	700
		$m_{u,2}$	1100
Suspension Linear Stiffness	N/m	$K_{s,1}$	0.4×10^6
		$K_{s,2}$	1×10^6
Suspension Viscous Damping	Ns/m	$C_{s,1}$	10×10^3
		$C_{s,2}$	20×10^3
Tyre Linear Stiffness	N/m	$K_{t,1}$	1.75×10^6
		$K_{t,2}$	3.5×10^6
Pitch Moment of Inertia	kg m ²	I_s	93 457
Distance of axle to centre of gravity, o	m	D_1	2.375
		D_2	2.375
Frequencies of vibration	Hz	Body bounce (y_s)	$f_{v,1}$ 1.00
		Body pitch (θ_s)	$f_{v,2}$ 1.55
		Axle 1 hop ($y_{u,1}$)	$f_{v,3}$ 8.83
		Axle 2 hop ($y_{u,2}$)	$f_{v,4}$ 10.21

The term $F_{t,i}$ in Eq. (2) represents the dynamic interaction force at wheel i :

$$F_{t,i} = K_{t,i}(y_{u,i} - w_{v,i}); i = 1,2 \quad (3)$$

where $w_{v,i}$ is the total displacement under wheel i and is defined in terms of the road profile displacement and bridge displacement under wheel i ; r_i and $w_{b,i}$ respectively, as follows:

$$w_{v,i} = w_{b,i} + r_i; i = 1,2 \quad (4)$$

For this investigation, only two on-vehicle acceleration measurement locations are utilised as input for the algorithm and these are indicated by the solid circles above the suspension of each axle in Figure 1. These measured sprung mass accelerations, $\ddot{y}_{s,i}$, are obtained from Eq. (5) using the sprung mass bounce and pitch rotation accelerations, \ddot{y}_s and $\ddot{\theta}_s$ respectively. These accelerations are contaminated with additive white gaussian noise with a signal-to-noise ratio (SNR) of 20 before they are used as input to the identification algorithm (Harris et al. 2010). This addresses the fact that in practice, the accuracy of measurements will be lower than in theoretical simulations due to errors such as random noise.

$$\ddot{y}_{s,i} = \ddot{y}_s - (-1)^i D_i \ddot{\theta}_s ; i = 1,2 \quad (5)$$

2.1.2 Bridge model

The simply supported FE beam which represents the bridge consists of 20 equally spaced elements with 21 nodes and two degrees of freedom per node, allowing for a vertical translation and rotation at each node and giving a total of $n = 42$ degrees of freedom. The response of this beam model to a series of time-varying forces can be written as:

$$\mathbf{M}_b \ddot{\mathbf{w}}_b + \mathbf{C}_b \dot{\mathbf{w}}_b + \mathbf{K}_b \mathbf{w}_b = \mathbf{N}_b \mathbf{f}_{\text{int}} \quad (6)$$

where \mathbf{M}_b , \mathbf{C}_b and \mathbf{K}_b are $(n \times n)$ global mass, damping and stiffness matrices of the beam model respectively, \mathbf{w}_b is the $(n \times 1)$ global vector of nodal bridge displacements and rotations and the product, $\mathbf{N}_b \mathbf{f}_{\text{int}}$, is the $(n \times 1)$ global vector of forces applied to the bridge nodes. The $(n_f \times 1)$ vector, $\mathbf{f}_{\text{int}} = \{P_1 + F_{t,1}, P_2 + F_{t,2}\}^T$, contains the total static plus dynamic interaction forces between the vehicle and the bridge. The matrix, \mathbf{N}_b , is an $(n \times n_f)$ location matrix that distributes the n_f applied interaction forces on beam elements to equivalent forces acting on the nodes; $n_f = 2$ for the two axle vehicle used in this paper. \mathbf{N}_b consists of zero entries and Hermitian shape function vectors and can be used to calculate the bridge displacement under each wheel, $w_{b,i}$, in Eq. (4) using:

$$\begin{Bmatrix} w_{b,1} \\ w_{b,2} \end{Bmatrix} = \mathbf{N}_b^T \mathbf{w}_b \quad (7)$$

Rayleigh damping is adopted for the beam, given by $\mathbf{C}_b = \alpha \mathbf{M}_b + \beta \mathbf{K}_b$. The damping constant ζ is assumed to be the same for the first two modes and the constants α and β are obtained from $\alpha = 2 \zeta \omega_1 \omega_2 / (\omega_1 + \omega_2)$ and $\beta = 2 \zeta / (\omega_1 + \omega_2)$ where ω_1 and ω_2 are the first two natural frequencies of the bridge (Yang et al. 2004). The properties of the three bridge spans used in theoretical simulations are given in Table 2 (González et al. 2011). The Young's Modulus, E , for all spans is $3.5 \times 10^{10} \text{ N/m}^2$.

Table 2 Finite element beam properties

Span Length, L (m)	Second moment of area, J (m ⁴)	Mass per unit length, μ (kg/m)	Damping constant, ζ	1st natural frequency of vibration, $f_{b,1}$ (Hz)
15	0.5273	28 125	0.03	5.66
25	1.3901	18 358	0.03	4.09
35	3.4162	21 752	0.03	3.01

2.1.3 Coupling of the vehicle and bridge

The vehicle and bridge models are coupled at the contact points of the vehicle wheels by the interaction force \mathbf{f}_{int} . Eqs. (1) and (6) are combined to form the coupled equations of motion shown in Eq. (8).

$$\mathbf{M}_g \ddot{\mathbf{u}} + \mathbf{C}_g \dot{\mathbf{u}} + \mathbf{K}_g \mathbf{u} = \mathbf{f} \quad (8)$$

\mathbf{M}_g and \mathbf{C}_g are the combined system mass and damping matrices respectively, \mathbf{K}_g is the coupled time-varying system stiffness matrix and \mathbf{f} is the system force vector. The vector, $\mathbf{u} = \{\mathbf{y}_v, \mathbf{w}_b\}^T$ is the displacement vector of the system. Eq. (8) is solved using the Wilson-Theta integration scheme in MATLAB and the optimal value of the parameter $\theta = 1.421$ is used for unconditional stability (Tedesco et al. 1999; Weaver and Johnston 1987).

2.1.4 Simulated road profiles

As the algorithm aims to identify road profile heights in addition to dynamic axle forces, a road profile is included in simulations for the coupled VBI model. The irregularities of this profile are randomly generated according to the ISO standard (ISO 8608 1995). Building upon the work by OBrien et al. (2012), five road profile types are investigated in this paper in order to examine the effect of a wider range of road roughness classes on the identification algorithm. The road profiles are: a class 'A' road (very good profile), class 'B' road (good), class 'C' road (average), class 'D' road (poor) and a class 'E' road (very poor), having geometric spatial means of 16×10^{-6} , 64×10^{-6} , 256×10^{-6} , 1024×10^{-6} and 4096×10^{-6} m³/cycle respectively. In reality, the tyre contact with the road is not an idealised 'point' contact. Therefore, a moving average filter is applied to the generated road profile heights, r_i , over a distance of 0.24 m to simulate the attenuation of short wavelength disturbances by a tyre contact 'patch' (Harris et al. 2007). A 100m approach length is also included in the road profile prior to the bridge span. As there is no bridge interaction as the vehicle travels along the approach profile (i.e., $w_{b,i} = 0$ in Eq. (4)), this road section will be the target in simulations to test the ability of the algorithm in identifying road profile height. The approach profile length of 100m is chosen in order to enable comparison of the computational runtime with the algorithm proposed by Harris et al. (2010),

2.2 Experimental Scenarios

The experimental setup in the laboratory consists of a scaled steel beam bridge model (Figure 2(a)) and a scaled two axle sprung mass vehicle model (Figure 2(b)). The vehicle is fitted with 2 accelerometers to monitor its bounce motion; at the centre of the front and rear axles respectively. It is also equipped with a wireless data acquisition system and strain sensors are used to monitor the vehicle entry and exit to the beam. The vehicle travels along a track on the beam which has a scaled rough road surface profile and its speed is maintained constant by an electronic controller. Three vehicle speeds are used in the experiment; $S1 = 0.46$ m/s,

$S2 = 0.93$ m/s and $S3 = 1.63$ m/s. The vehicle can be adjusted to obtain different axle configurations and dynamic properties. In this experiment, two vehicle configurations are used with the properties given in Table 3. The axle spacing and track width for all models are 0.4 m and 0.2 m respectively. The sprung mass bounce frequencies of vehicles V1 and V2 are 2.93 Hz and 3.62 Hz respectively while the sprung mass pitch frequencies are 4.24 Hz (V1) and 5.35 Hz (V2).

Table 3 Experimental vehicle model properties

Vehicle	Mass (kg)		Suspension stiffness (N/m)		Suspension damping (N s/m)	
	Axle 1	Axle 2	Axle 1	Axle 2	Axle 1	Axle 2
V1	7.9	13.45	2680	4570	16.01	27.76
V2	7.9	13.45	4290	7310	13.99	35.11

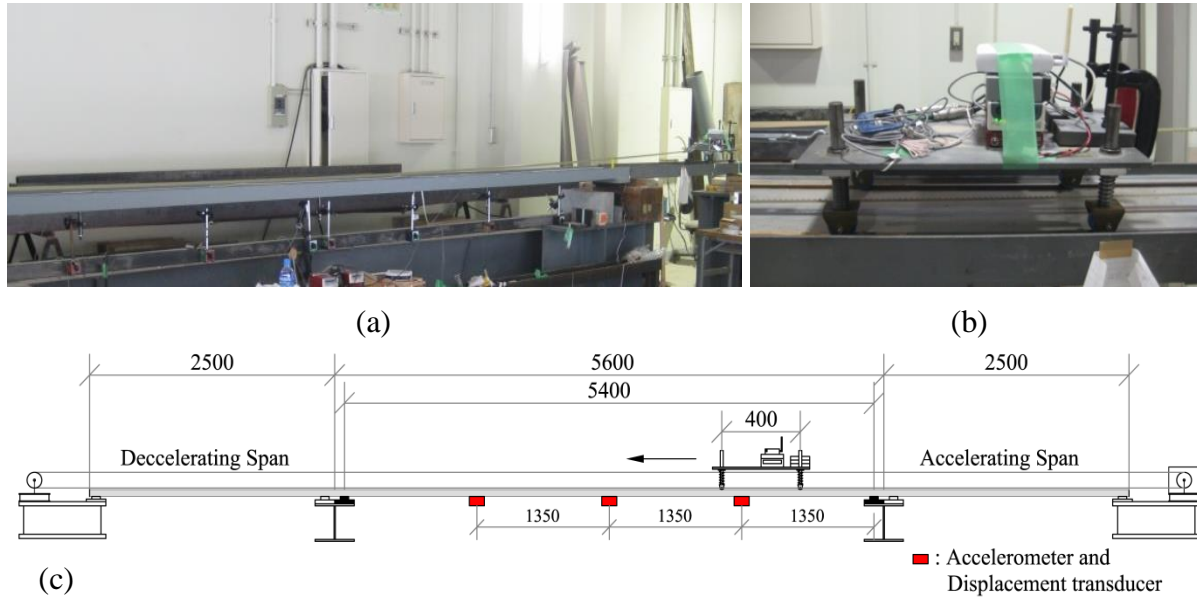


Figure 2. (a) Experimental Beam (b) Experimental Vehicle (c) Elevation of setup

The bridge model is a simply supported steel beam with a span length, L_{exp} , of 5.4 m. The beam properties are obtained from the manufacturer and free vibration tests. It has a Modulus of Elasticity, E_{exp} , of 200×10^9 N/m² and mass per unit length, μ_{exp} , of 52.26 kg/m. Its first natural frequency is 2.7 Hz and the damping constant is 0.016. The beam is fitted with accelerometers and displacement transducers at quarter span, mid span and three-quarter span to monitor its vibration. However, only the sensors in the vehicle are used to infer the road profile. An elevation of the experimental setup is shown in Figure 2(c). The scaled road profile on the beam which the vehicles travel along is shown in Figure 3. The sampling frequency used in all experiments is 100 Hz.

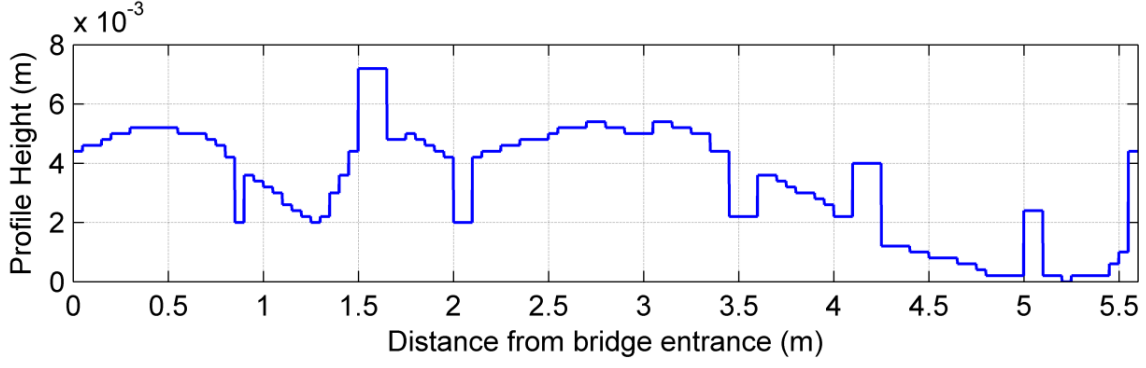


Figure 3. Experimental road profile

2.3 Force Identification Algorithm

The force identification algorithm investigated in this paper has been adapted from the MFI algorithm described in detail by González et al. (2008b) and further details of the implementation discussed here can be found in McGetrick (2012) and OBrien et al. (2012). Therefore, the main features of the algorithm are summarised in this paper. A flowchart summarising the algorithm inputs, outputs and processes is presented in Figure 4. The forces to be identified are contained in the vector, $\mathbf{g}_j = \{-F_{t,1}, -F_{t,2}\}^T$.

In part 1 of the algorithm flowchart, acceleration measurements taken on the vehicle are represented by the $(m \times 1)$ vector, \mathbf{d}_j . In practice, the number of measurements taken on a vehicle, m , will be much less than the total number of degrees of freedom but greater than or equal to the number of forces, n_f . For the theoretical vehicle model in this paper, two acceleration measurements are taken ($m = 2$) which is equal to the number of forces n_f but corresponds to only half of the total vehicle degrees of freedom (4). In simulations, ‘measured’ accelerations, $\mathbf{d}_j = \{\ddot{y}_{s,1}, \ddot{y}_{s,2}\}^T$, are generated using the model outlined in Section 2.1.1 while in the laboratory experiment, the ‘measured’ accelerations are those recorded from accelerometers on the scaled vehicle model (Figure 2(b)). To allow the formulation of the algorithm, these m acceleration measurements must be related to the vehicle model state space variables, $\hat{\mathbf{X}}_j$, (Eq. (9)) using a selection matrix \mathbf{Q} ; $\mathbf{d}_j = \mathbf{Q}\hat{\mathbf{X}}_j$.

In Figure 4, part 2 of the flowchart involves state space formulation of the vehicle equations of motion for solving using the Dynamic Programming (DP) technique in part 5. The state space formulation of the vehicle equations can be converted into a first order system using the exponential matrix representation shown in Eq. (9). The forces to predict are included in the (10×1) state variable vector $\hat{\mathbf{X}}_j = \{\mathbf{X}_j \ \mathbf{g}_j\}^T$, where $\mathbf{X} = \{\mathbf{y}_v \ \dot{\mathbf{y}}_v\}^T$ and the vector \mathbf{r}_j contains the derivative of the forces.

$$\hat{\mathbf{X}}_{j+1} = \begin{bmatrix} \mathbf{M} & \mathbf{G} \\ 0 & \mathbf{I} \end{bmatrix} \hat{\mathbf{X}}_j + \begin{bmatrix} 0 \\ \mathbf{I} \end{bmatrix} \mathbf{r}_j; \quad j = 1, \dots, N \quad (9)$$

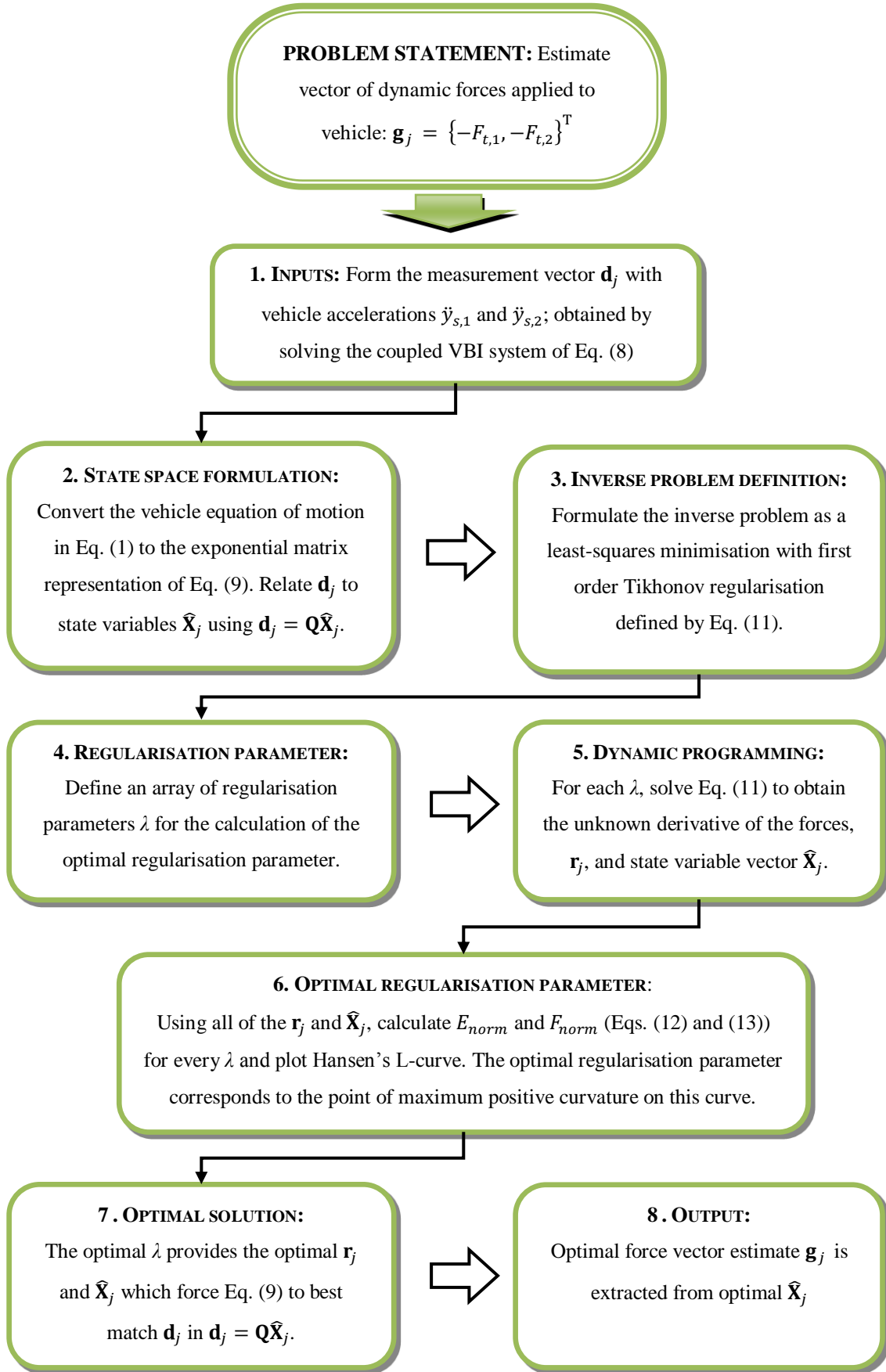


Figure 4. Force identification algorithm

where the scalar, N , is the total number of discrete measurements. In Eq. (9), $\mathbf{M} = e^{\mathbf{A}h}$ for time step h with \mathbf{A} and \mathbf{G} defined by Eq. (10);

$$\mathbf{A} = \begin{bmatrix} 0 & \mathbf{I} \\ -\mathbf{M}_v^{-1}\mathbf{K}_v & -\mathbf{M}_v^{-1}\mathbf{C}_v \end{bmatrix}, \quad \mathbf{G} = (\mathbf{A}^{-1}(\mathbf{M} - \mathbf{I})) \begin{bmatrix} \mathbf{0} \\ \mathbf{M}_v^{-1}\mathbf{L}_v \end{bmatrix} \quad (10)$$

where $\mathbf{L}_v = [\mathbf{0} \quad \mathbf{I}]^T$ is a (4×2) location sub-matrix.

The inverse problem of the algorithm in part 3 uses first order Tikhonov regularisation (Tikhonov and Arsenin 1977) and can be formulated as a non-linear least squares minimisation of the difference between measured and theoretical vehicle accelerations, represented by the error sum given in Eq. (11). This problem aims to find the optimal unknown derivative of the forces \mathbf{r}_j which when used in Eq. (9) forces the system to best match the acceleration measurements.

$$Err(\hat{\mathbf{X}}_k, \mathbf{r}_k) = \sum_{k=1}^m (\mathbf{d}_k - \mathbf{Q}\hat{\mathbf{X}}_k, \mathbf{W}(\mathbf{d}_k - \mathbf{Q}\hat{\mathbf{X}}_k)) + (\mathbf{r}_k, \mathbf{B}\mathbf{r}_k) \quad (11)$$

In Eq. (11), \mathbf{W} is an $(m \times m)$ identity matrix and (\mathbf{x}, \mathbf{y}) denotes the vector product of \mathbf{x} and \mathbf{y} , i.e., for terms corresponding to measurement k , $(\mathbf{x}_k, \mathbf{y}_k) = \sum_{j=1}^N \mathbf{x}_{k,j} \mathbf{y}_{k,j}$. The $(n_f \times n_f)$ diagonal matrix \mathbf{B} contains the optimal regularisation parameter λ ($\mathbf{B} = \lambda \mathbf{I}$). The addition of the regularisation term here allows control of the smoothness in the solution by varying the regularisation parameter.

For the vehicle model described in Section 2.1.1, the number of measurements m is less than the total number of degrees of freedom of the vehicle and the inverse problem is ill-conditioned. This means that small changes in the vector \mathbf{d}_j or the matrix \mathbf{Q} can cause significant fluctuations in the solution vector $\hat{\mathbf{X}}_j$. The addition of the regularisation parameter λ to the least squares error in Eq. (11) improves the conditioning of the inverse problem and hence reduces the error in the solution. In first order Tikhonov regularisation, the derivative of the unknown forces, \mathbf{r}_j , is regularised and this provides a smoother solution than a zeroth order system (Busby and Trujillo 1997, González et al. 2008b). Here, the DP technique (Trujillo 1978) is used to solve the least squares minimisation problem of Eq. (11) for a value of λ , corresponding to part 5 of Figure 4. The DP technique is effectively a recurrence algorithm and it is a very efficient method that may be used to solve large least squares problems such as that of Eq. (11) and others encountered in MFI.

In part 6 of Figure 4 the optimal value for λ is obtained using Hansen's L-Curve (Hansen 1992, Busby and Trujillo 1997). The method is described in detail by González et al. (2008b). The L-curve is plotted on a log-log scale using the residual least squares norm (E_{norm}) and solution norm (F_{norm}), given in Eqs. (12) and (13) respectively:

$$E_{norm} = \sqrt{\sum_{k=1}^m (\mathbf{d}_k - \mathbf{Q}\hat{\mathbf{x}}_k, \mathbf{W}(\mathbf{d}_k - \mathbf{Q}\hat{\mathbf{x}}_k))} \quad (12)$$

$$F_{norm} = \sqrt{\sum_{k=1}^m (\mathbf{r}_k, \mathbf{r}_k)} \quad (13)$$

The optimal value for λ corresponds to the point of maximum positive curvature on the L-curve plot. This λ value is selected to provide the optimal force vector estimate (parts 7 and 8 in Figure 4).

2.4 Road Profile Identification

The methodology of the force identification algorithm presented in Section 2.3 allows for the simultaneous prediction of pavement roughness. In the force identification algorithm, the vector of forces, \mathbf{g}_j , is identified for the optimal regularisation parameter. This vector contains the dynamic forces applied to the vehicle, $F_{t,1}$ and $F_{t,2}$ defined by Eq. (3). The axle displacements $y_{u,i}$ are also predicted in \mathbf{y}_v as part of the state variable vector, $\hat{\mathbf{x}}_j$. If the tyre stiffness $K_{t,i}$ is known for each tyre i , the estimated displacement under wheel i , $w_{v,i}$, can be obtained from Eq. (3). If the algorithm is used to identify the vehicle forces due to road pavement excitation only, for example, when it travels along the 100 m approach length (i.e., $w_{b,i} = 0$ in Eq. (4)), then $w_{v,i} = r_i$ ($i = 1,2$) is effectively a prediction of the road profile height under wheel i . Therefore, in one run, both the axle forces and road profile heights can be estimated simultaneously using this approach. In this paper, only the road profile heights identified along the 100m approach length are presented for simulations. However, in the experiment, profile heights identified along the bridge are presented as they are an important part of the VBI. In total for one run, the algorithm only requires a computational time of 30 seconds on average with a 3.4GHz processor and 4GB RAM running in MATLAB which is significantly faster than the time noted for the algorithm proposed by Harris et al. (2010).

3. RESULTS AND DISCUSSION

3.1 Theoretical Testing

This section presents the results obtained from testing the algorithm with theoretical simulations based on the coupled VBI model of Section 2.1. To provide a comparative measure of accuracy between results for the force identification algorithm, the Root Mean Square Error (RMSE) between the identified and true dynamic forces is used. The RMSE of the identified dynamic forces is calculated and expressed as a percentage of the maximum absolute true dynamic force magnitude. Also, all analysis of the identified 100m long road profiles is carried out using Profile Viewing and AnaLysis (ProVAL) (Chang et al. 2006).

3.1.1 Axle force identification

The acceleration responses obtained from the coupled VBI model are contaminated with noise having a SNR of 20. **Error! Reference source not found.** illustrates an example of the original and noise contaminated simulated accelerations obtained above axle 1 of the vehicle as it crosses the 25 m bridge span. **Error! Reference source not found.** shows the dynamic axle forces identified from the contaminated acceleration measurements above both axles using the algorithm.. It can be seen that the algorithm is able to capture the main features of the applied forces. However, due to the smoothing of the solution by the regularisation terms, some of the higher frequency components of the forces are not identified correctly. It can be seen that the larger amplitude components of the applied forces are identified with a high level of accuracy. These peaks are an important factor with respect to damage and deterioration of pavements and bridges as they can indicate specific locations in pavements where the damage will be concentrated (Cole and Cebon 1992).

Table 4 presents the RMSE of the identified forces expressed as a percentage of the maximum absolute true dynamic force magnitude. It should be noted that these values are percentages of the dynamic increment of the axle forces only; the much larger static force components are not considered here. The percentage RMSEs are given for each bridge span and road profile investigated. The errors observed in this table are predominantly consequences of the presence of high frequency components in the true dynamic axle force history which are not identified very well. However, the errors are generally less than 10% and similar accuracy is obtained for each bridge span and axle force. The values in this table suggest that the identified forces are not very sensitive to the road roughness as there are only slight variations in error as the roughness level increases. The mean of all values is 7.77% with a standard deviation of 1.49%.

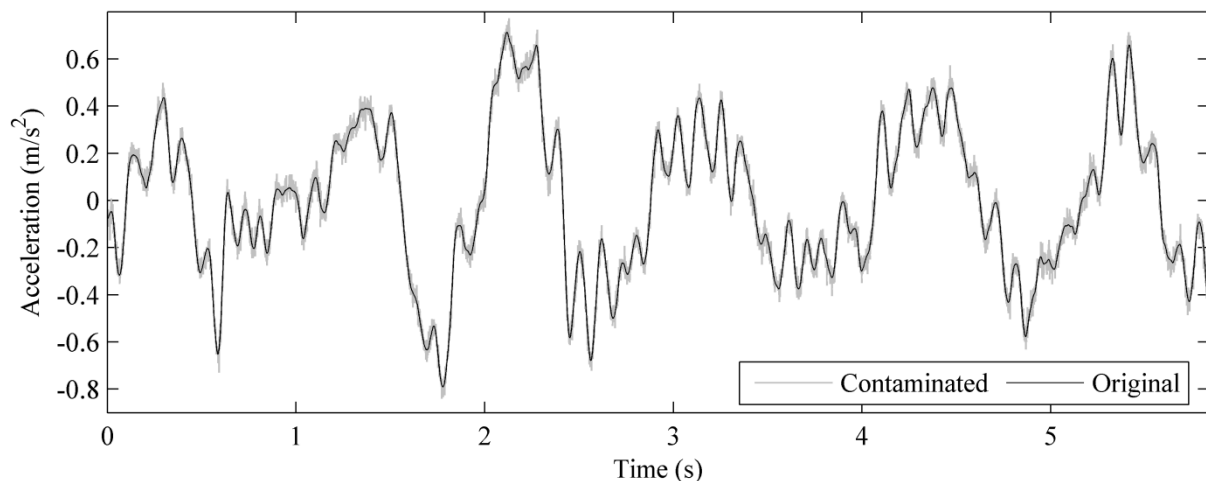


Figure 5. Measured accelerations, $\ddot{y}_{s,1}$, above axle 1 of vehicle crossing 25 m bridge and a class A profile.

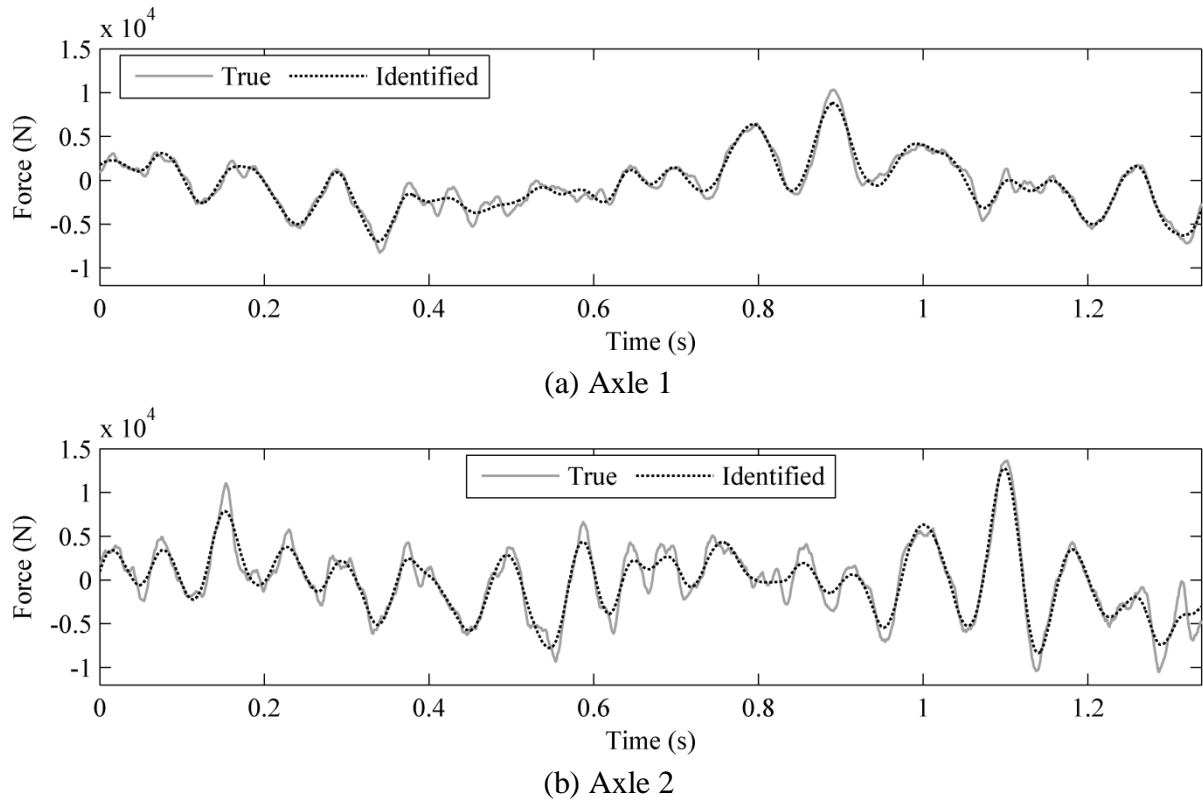


Figure 6. Dynamic axle forces of vehicle crossing 25 m bridge and a class A profile.

Table 4 Percentage RMSE of identified dynamic axle forces

Profile Class	RMSE (%)						
	15 m Span		25 m Span		35 m Span		Mean
	Axle 1	Axle 2	Axle 1	Axle 2	Axle 1	Axle 2	
A (very good)	8.15	5.65	6.18	8.32	9.62	7.31	7.54
B (good)	8.11	8.38	9.86	8.7	6.36	7.34	8.13
C (average)	11.46	6.38	8.51	5.99	6.03	5.2	7.26
D (poor)	7.74	6.23	8.63	7.21	7.51	7.98	7.55
E (very poor)	9.51	5.99	10.12	8.22	7.51	8.97	8.39

3.1.2 Road profile height identification

The results of road profile height identification using the algorithm are presented in this section. As each wheel passes over the same road profile, the identified profile will be the same under each wheel, with the profile under wheel 2 shifted from that under wheel 1 by the

vehicle axle spacing of 4.75 m. Hence, only the results of the profile identification under wheel 2 are provided here for the 100m profiles.

The results of road profile identification for the 100m class A profile are presented in **Error! Reference source not found.** The prediction is very good overall. However, similar to the identified forces in the previous section, it can be seen that some of the very small amplitude higher frequency irregularities are not identified. This is particularly clear from the Power Spectral Density (PSD) of the profile heights shown in **Error! Reference source not found.**(b).

Error! Reference source not found. to **Error! Reference source not found.** show the identified road profile heights and corresponding spectra for the four other profiles investigated, class B, C, D and E respectively. In general, the accuracy is similar to that for the class A profile and does not appear to vary significantly with increasing road roughness. From these figures, it can be observed that the algorithm is less accurate in the characterisation of higher frequency components and some very low frequency components. However, it can be inferred that all identified profiles, including the class A profile, more accurately characterise the true profiles for the frequency band between 0.02 cycles/m and 1 cycles/m approximately.

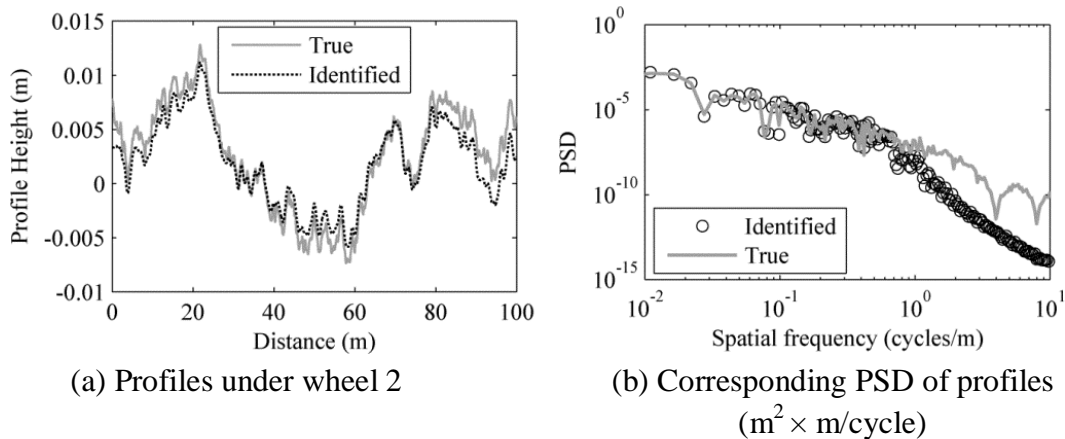


Figure 7. Profile heights for ISO class A profile identified using acceleration measurements

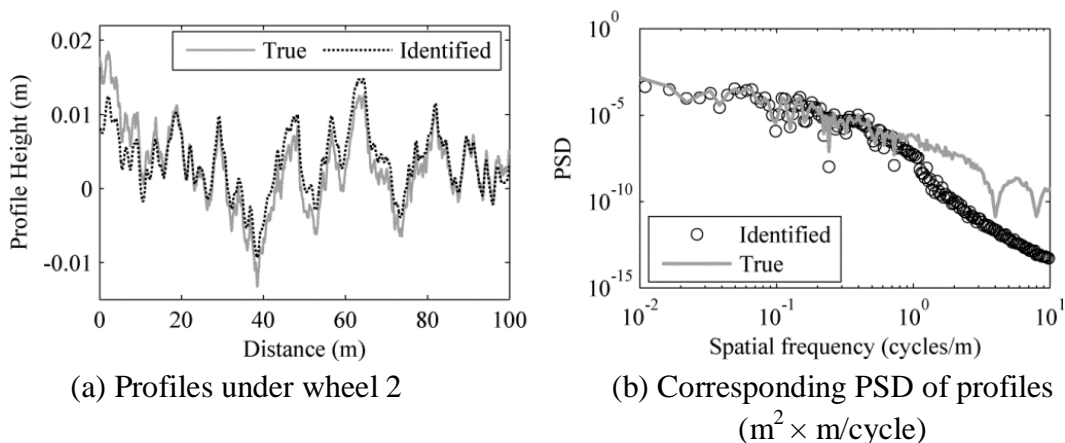


Figure 8. Profile heights for ISO class B profile identified using acceleration measurements

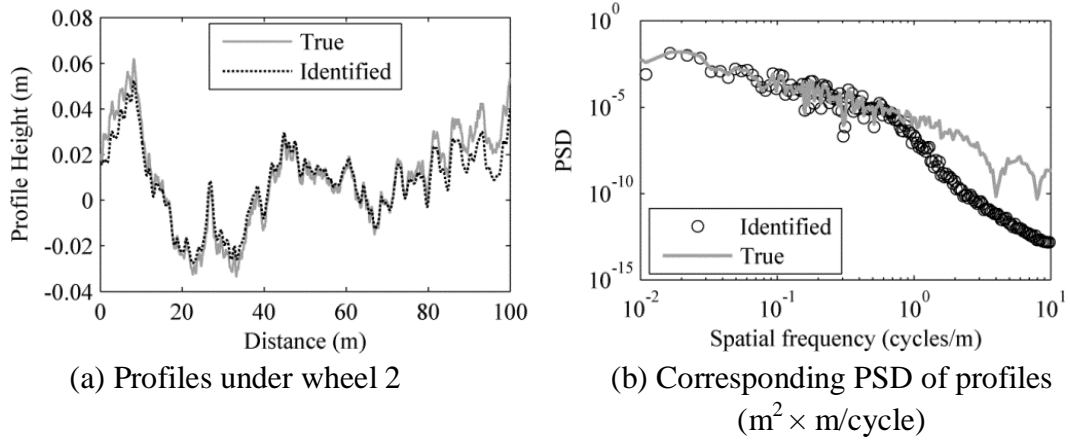


Figure 9. Profile heights for ISO class C profile identified using acceleration measurements

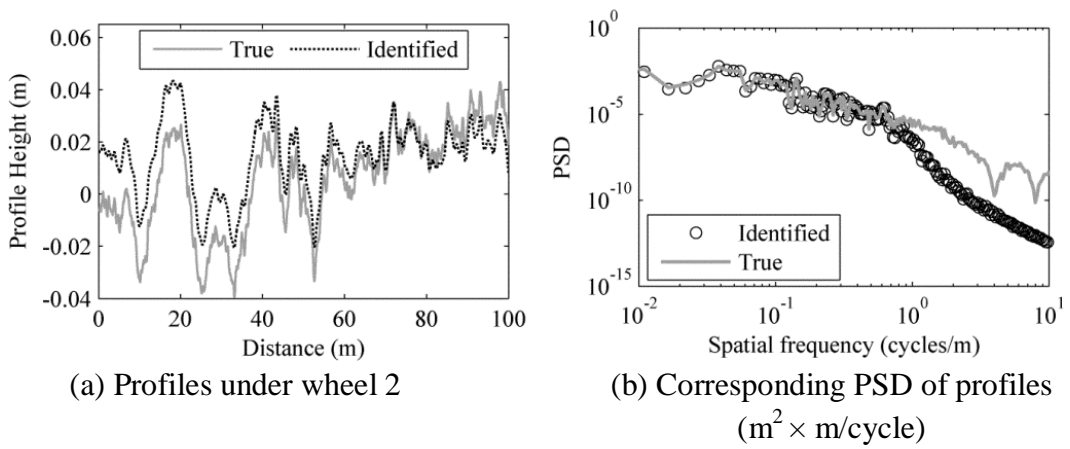


Figure 10. Profile heights for ISO class D profile identified using acceleration measurements

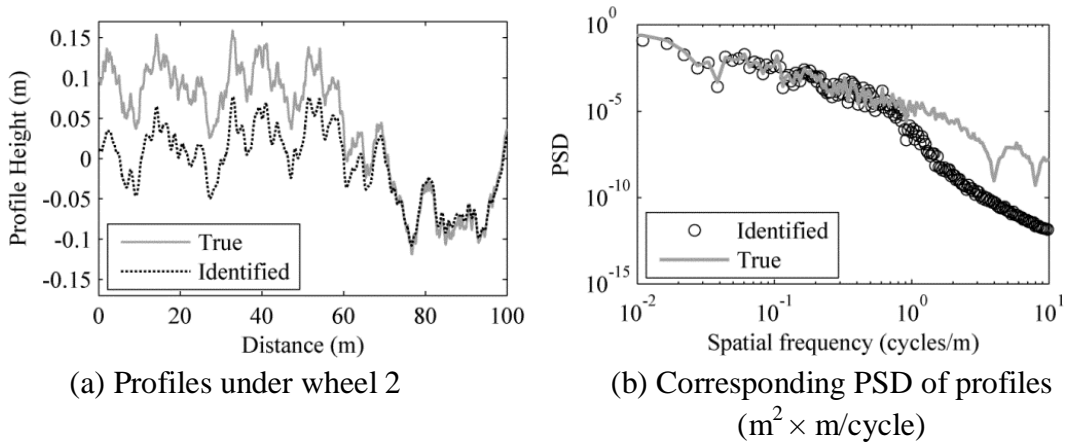


Figure 11. Profile heights for ISO class E profile identified using acceleration measurements

The IRI values of all profiles predicted using acceleration measurements are presented in Table 5. The true IRI values and percentage errors are also tabulated. There is not a noticeable trend in accuracy with increasing road profile roughness. However the errors are all less than 8% and the identified profiles underestimate the IRI values. This relates to the poor estimation of higher frequency and some lower frequency components of the road profile.

Table 5 IRI of true and identified road profile heights under wheel 2 on 100m profile

Profile Class	IRI (m/km)		
	True	Identified	% Error
A (very good)	1.99	1.83	8.0
B (good)	4.01	3.83	4.5
C (average)	9.47	8.82	6.9
D (poor)	10.66	10.01	6.1
E (very poor)	28.16	26.2	7.0

3.2 Experimental Testing

The simulations allow for numerical validation of the algorithm for a wide range of parameters. However, to assess the effectiveness of the algorithm in a more realistic environment, it is also applied to the acceleration measurements obtained from a laboratory experiment and the results of this experimental study are presented in this section. Due to the experimental setup, the measurements are more conducive to identification of road profile heights on the bridge. Therefore these profile heights (Figure 3) are the focus of this section.

3.2.1 Road profile height identification

The results of the experimental road profile identification for wheel 2 of vehicle model V1 are presented in **Error! Reference source not found.** for all speeds investigated. In the identified profiles, ‘drift’ was apparent due to low frequency inaccuracies. A linear correction has therefore been made in **Error! Reference source not found.** to the identified profiles, i.e., the profile elevations at the start and end of the bridge were adjusted to give the same value. These figures show that both the larger road irregularities and the bridge displacement profile underneath the wheel are picked up by the algorithm when applied to accelerations measured while crossing the bridge. Also, it can be observed that as the speed increases, the ability of the algorithm to detect higher frequency components decreases due to the increase in spatial sampling step. Furthermore, for speed S3, the bridge displacement profile is overestimated compared to speeds S1 and S2, suggesting that lower speeds are more suitable for this type of approach.

The corresponding profile spectra for vehicle V1 are plotted in **Error! Reference source not found.** The resolutions of the spectra are 0.106 cycles/m, 0.105 cycles/m and 0.12 cycles/m here for speeds S1, S2 and S3 respectively due to the sampling frequency of the experiment (100 Hz). This figure highlights that despite the varying spectral resolutions, similar accuracy is obtained for each speed. However, speed S3 (**Error! Reference source not found.**(c)) displays more significant errors at low frequencies and near frequencies close to 10 cycles/m.

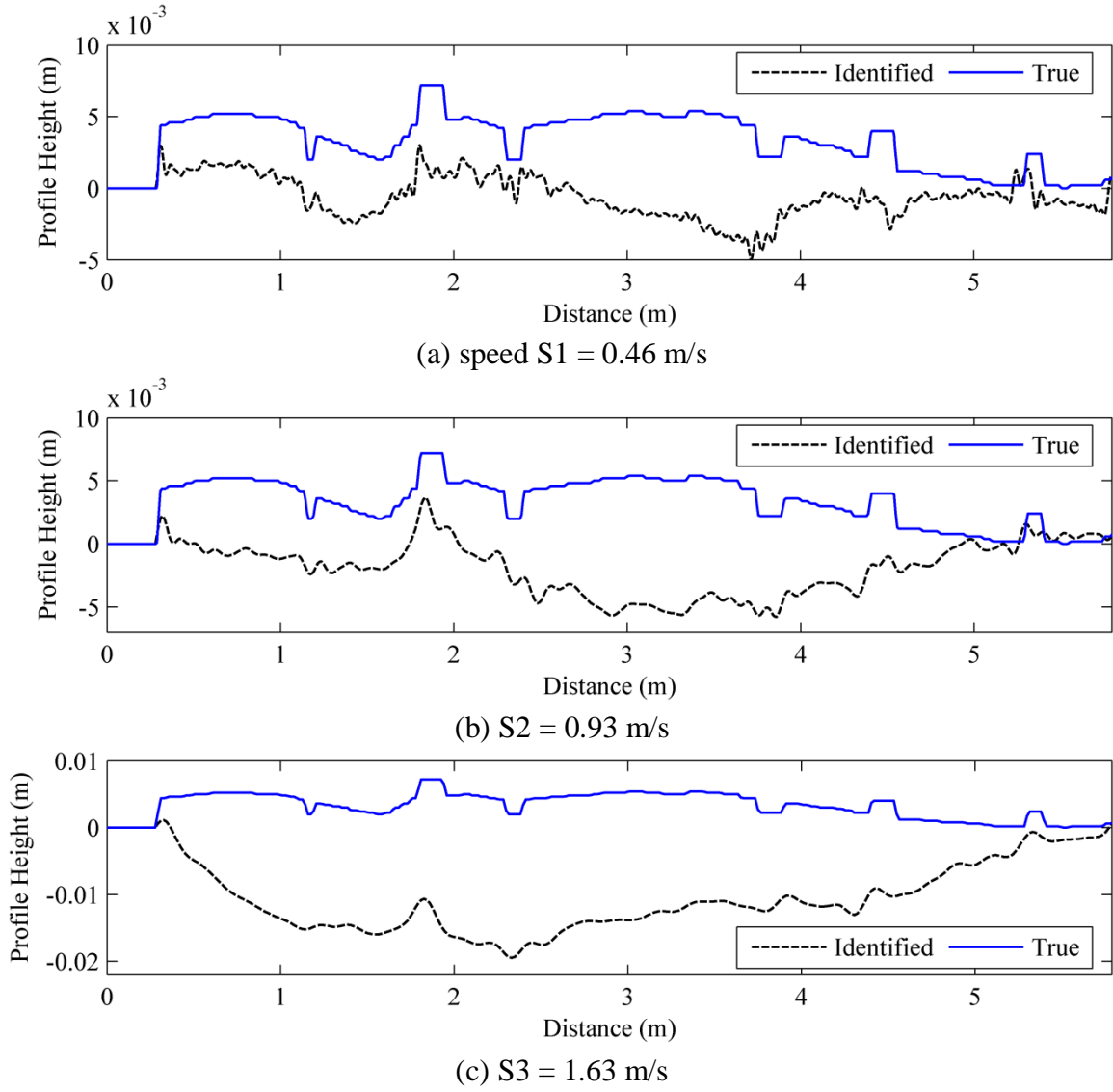


Figure 12. Identified road profile heights from experiment under wheel 2 of vehicle V1

Although the results are less accurate than those in simulations, they indicate that this approach can detect the larger road profile irregularities, which can indicate locations susceptible to the concentration of damage. The overall accuracy seems to be influenced by the initial conditions of the vehicle model and the sampling frequency of 100 Hz.

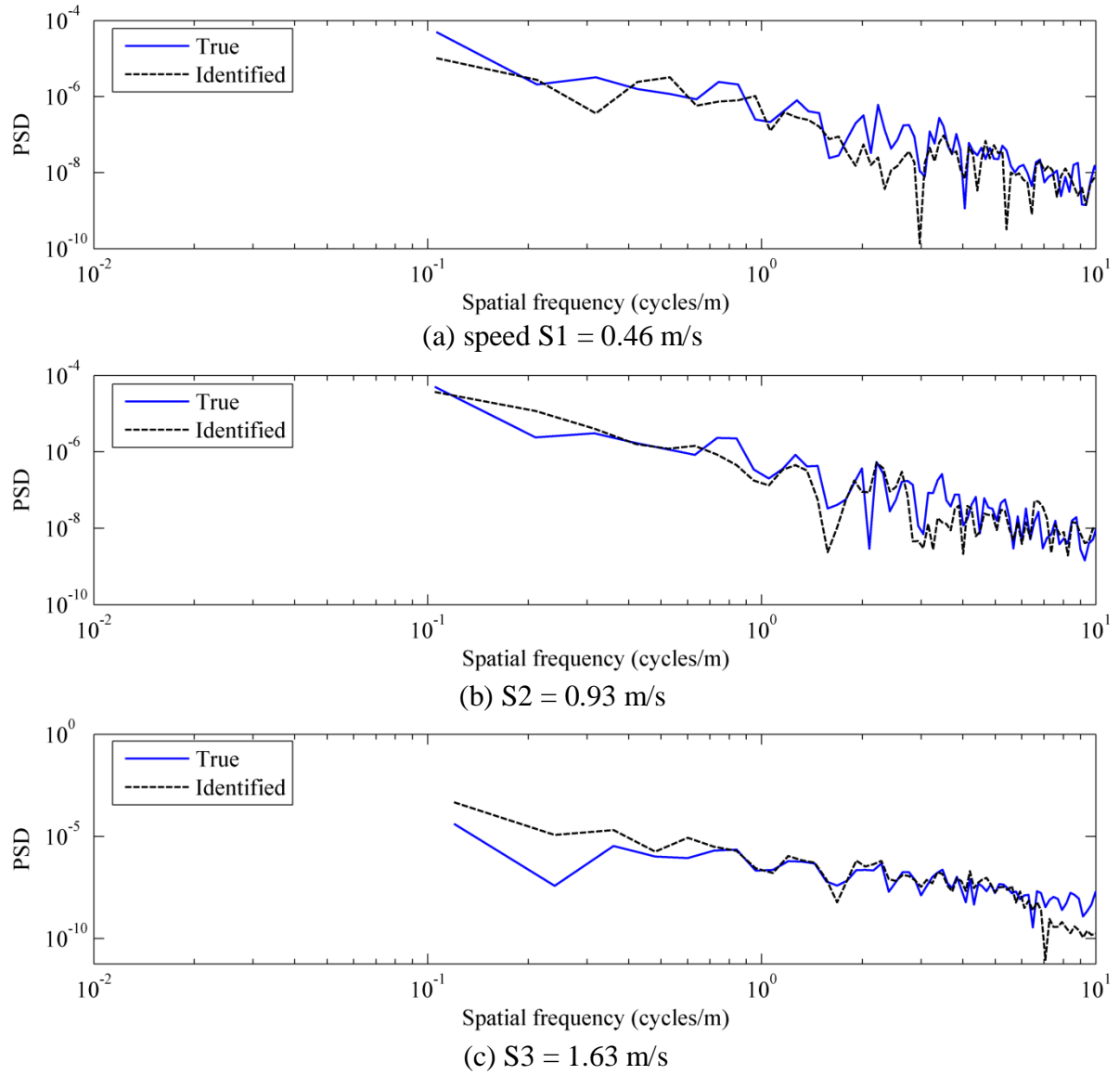


Figure 13. PSD ($\text{m}^2 \times \text{m/cycle}$) of profile heights under wheel 2 of vehicle V1

Error! Reference source not found. shows the identified road profile heights under wheel 2 of experimental vehicle V2 for all speeds investigated. Their corresponding spectra are shown in **Error! Reference source not found.**. The resolutions of the spectra are the same as those in **Error! Reference source not found.**. From these figures it can be ascertained that while the accuracy for vehicle V2 and speed S1 (**Error! Reference source not found.**(a)) is comparable to that observed for vehicle V1 (**Error! Reference source not found.**(a)), the identified profiles for vehicle V2 at speeds S2 and S3 are less accurate than the corresponding profiles identified for V1. Also, for speed S3 the bridge displacement is not identified very well and the spectra are more accurate for V1 than V2. Nevertheless, **Error! Reference source not found.** shows that despite the accuracy decreasing with increasing speed, the larger road irregularities are detected by the algorithm at all speeds.

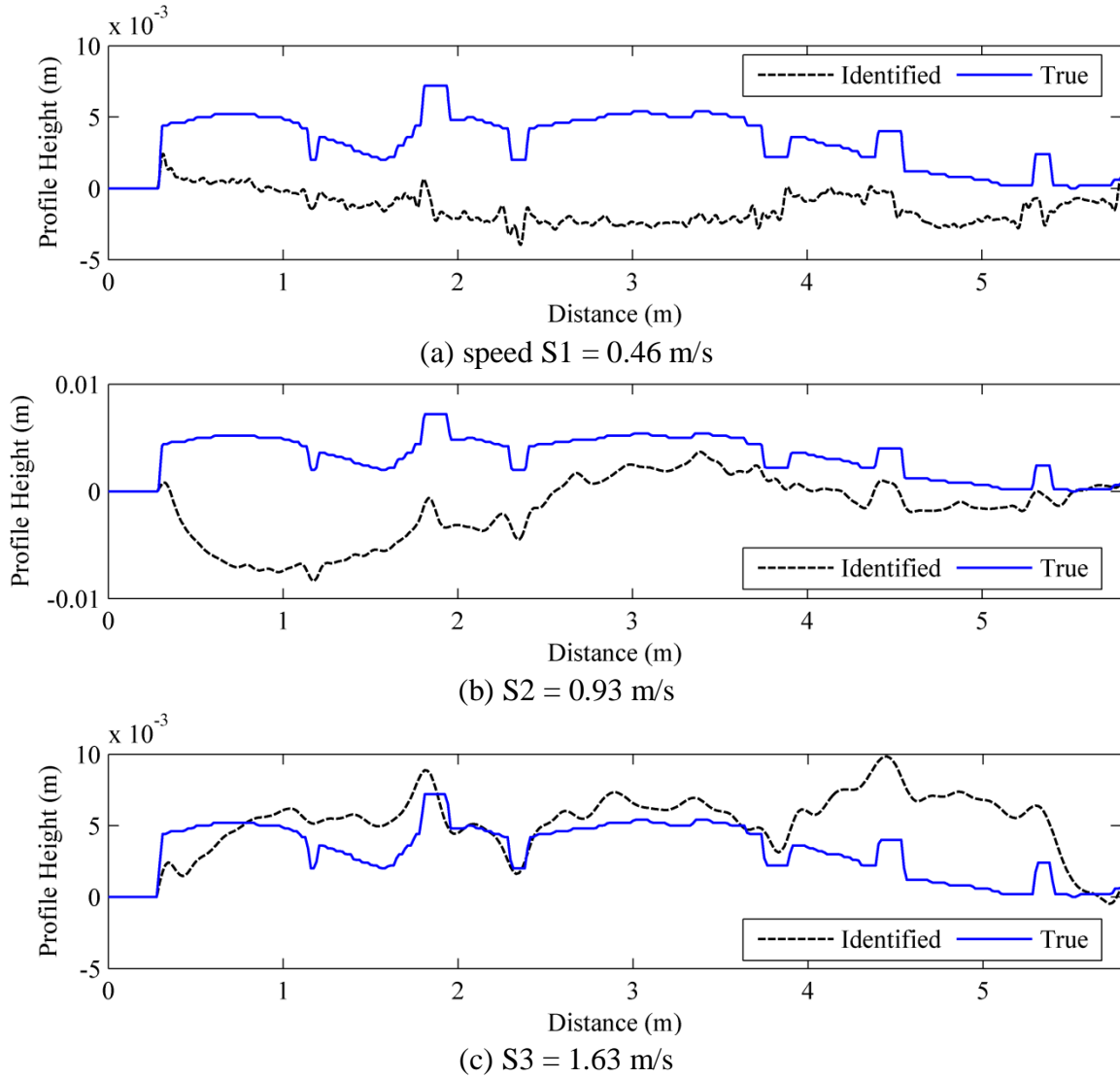


Figure 14. Identified road profile heights from experiment under wheel 2 of vehicle V2

These results indicate that of all the vehicle configurations and speeds tested, vehicle V1 and lower speeds provide the best opportunity to identify the road profile heights (which include the bridge displacement profile here) underneath the wheel from measured accelerations. This may be due to vehicle V1 having a sprung mass bounce frequency (2.93 Hz) which is closer to the first natural frequency of the beam (2.7 Hz) than that of vehicle V2 (3.62 Hz), which allows a more accurate determination of the bridge component of the profile identified under the wheel.

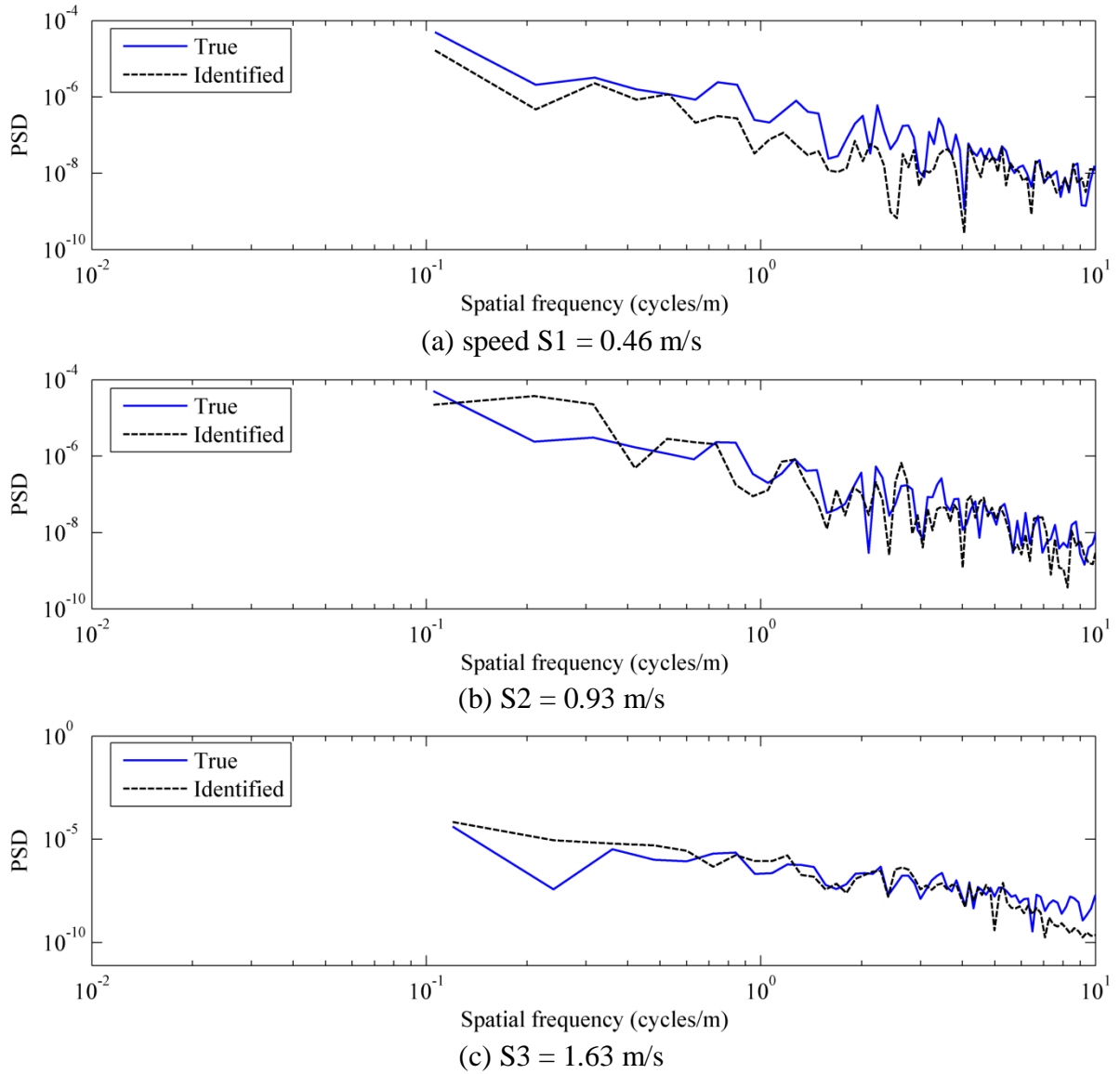


Figure 15. PSD ($\text{m}^2 \times \text{m/cycle}$) of profile heights under wheel 2 of vehicle V2

4. CONCLUSIONS

This paper has presented the results of a novel algorithm which utilizes MFI theory for the identification of dynamic axle forces and road profile heights from a vehicle's acceleration response. In a theoretical investigation, it has been found that the algorithm is able to identify the vehicle's dynamic axle forces as it crossed different bridge spans with reasonable accuracy. The accuracy of the predicted forces has been found to be insensitive to road roughness. The algorithm identified road profile heights of varying roughness quite accurately also in a 100m long road, with an average IRI error of 6.5%.

In a laboratory experiment, the algorithm has been applied to the accelerations of a scaled vehicle model crossing a scaled artificial road profile along a 5.4 metre steel beam. While in a full scale field experiment the algorithm would have needed to deal with a limited number of

measurements, both degrees of freedom of the vehicle model have been measured in the laboratory experiment. The results indicate that this approach can detect larger road profile irregularities which can indicate locations susceptible to damage. It is found that lower speeds provide higher accuracy. However, the initial conditions of the vehicle and bridge deflections have prevented accurate identification of the entire road profile spectrum for some speeds tested. Overall this paper has illustrated the potential of this approach to be developed and implemented as a low-cost tool for identifying dynamic vehicle axle forces and the condition monitoring of pavements.

5. ACKNOWLEDGEMENTS

The authors wish to express their gratitude for the financial support received towards this investigation from the Japanese Society for the Promotion of Science Postdoctoral Fellowship for North American and European Researchers (Short Term), from the 7th European Framework ASSET (Advanced Safety and Driver Support in Efficient Road Transport) project and also from the Japanese Society for the Promotion of Science for the Grant-in-Aid for Scientific Research (B) under project no. 24360178. The authors also wish to express their gratitude to Prof. M. Kawatani and Mr. T. Toshinami for their support and assistance during the experimental investigation.

6. REFERENCES

- Busby, H.R. and Trujillo, D.M. (1997). "Optimal regularization of an inverse dynamics problem". *Computers and Structures*, 63(2), 243–248.
- Cebon, D. (1987). "Assessment of the dynamic wheel forces generated by heavy road vehicles". *Proceedings of ARRB/FORS Symposium on Heavy vehicle suspension characteristics*, Canberra, Australia, 143–162.
- Cebon, D. (1999). *Handbook of vehicle-road interaction*. Swets and Zeitlinger Publishers, Lisse, The Netherlands.
- Chang, G.K., Dick, J.C. and Rasmussen, R.O. (2006). *ProVAL Users guide*. The Transtec Group, Inc.
- Cole, D.J. and Cebon, D. (1992). "Spatial repeatability of dynamic tyre forces generated by heavy vehicles". *Proceedings of the Institution of Mechanical Engineers*, Part D, 206(D1), 17–27.
- DAF Trucks Limited (2011). *FA LF55 18t Specification sheet*, DAF Trucks Limited.
- Davis, L. and Bunker, J. (2007). *Heavy Vehicle Suspensions – Testing and Analysis. A literature review*. Brisbane, Queensland: Queensland Department of Main Roads, Queensland University of Technology, Australia.
- Deng, L. and Cai, C.S. (2010b). "Identification of Dynamic Vehicular Axle Loads: Theory and Simulations". *Journal of Vibration and Control*, 16(14), 2167–2194.

- González, A., OBrien, E.J., Li, Y.-Y. and Cashell, K. (2008a). "The use of vehicle acceleration measurements to estimate road roughness". *Vehicle System Dynamics*, 46(6), 483–499.
- González, A., Rowley, C. and OBrien, E.J. (2008b). "A general solution to the identification of moving vehicle forces on a bridge". *International Journal of Numerical Methods in Engineering*, 75(3), 335–354.
- González, A., OBrien, E.J. and McGetrick, P.J. (2010). "Detection of Bridge Dynamic Parameters Using an Instrumented Vehicle". *Proceedings of the Fifth World Conference on Structural Control and Monitoring*, Tokyo, Japan, paper 34.
- González, A. (2010). "Vehicle-bridge dynamic interaction using finite element modelling". In: David Moratal (Ed.). *Finite Element Analysis*. Sciyo, Croatia, 637–662.
- González, A., Cantero, D., OBrien, E.J. (2011). "Dynamic increment for shear force due to heavy vehicles crossing a highway bridge". *Computers and Structures*, 89(23–24), 2261–2272.
- Hansen, P.C. (1992). "Analysis of discrete ill-posed problems by means of the L-curve". *SIAM Review*, 34(4), 561–580.
- Harris, N.K., OBrien, E.J. and González, A. (2007). "Reduction of bridge dynamic amplification through adjustment of vehicle suspension damping". *Journal of Sound and Vibration*, 302(3), 471–485.
- Harris, N.K., González, A., OBrien, E.J. and McGetrick, P.J. (2010). "Characterisation of pavement profile heights using accelerometer readings and a combinatorial optimisation technique". *Journal of Sound and Vibration*, 329, 497–508.
- International Organization for Standardization ISO (1995). *Mechanical vibration – Road surface profiles - Reporting of measure data, ISO8608 (BS7853:1996)*.
- Kitching, J., Cole, D.J. and Cebon, D. (2000). "Theoretical investigation into the use of controllable suspensions to minimize road damage". *Proceedings of the Institution of Mechanical Engineers, Part D: Journal of Automobile Engineering*, 214, 13–31.
- Law, S.S., Chan, T.H.T. and Zeng, Q.H. (1997). "Moving force identification: a time domain method". *Journal of Sound and Vibration*, 201, 1–22.
- Law, S.S., Chan, T.H.T., Zhu, X.Q. and Zeng, Q.H. (2001). "Regularization in moving force identification". *Journal of Engineering Mechanics (ASCE)*, 127(2), 136–148.
- Law, S.S., Bu, J.Q., Zhu, X.Q. and Chan, S.L. (2004). "Vehicle axle loads identification using finite element method". *Engineering Structures*, 26, 1143–1153.
- McGetrick, P.J. (2012). *The Use of an Instrumented Vehicle to Monitor Transport Infrastructure*. PhD Thesis, University College Dublin, Ireland.
- OBrien, E.J., González, A. and McGetrick, P.J. (2012). "A drive-by inspection system via vehicle moving force identification". *Smart Structures and Systems*, accepted for publication.
- Sayers, M.W. and Karamihas, S.M. (1996). *Interpretation of road profile roughness data*. University of Michigan Transportation Research Institute, UMTRI-96-19.
- Sayers, M.W. and Karamihas, S.M. (1998). *The little book of profiling*. University of Michigan Transportation Research Institute, UMTRI-96-19.
- Tedesco, J.W., McDougal, W.G. and Ross, C.A. (1999). *Structural Dynamics, Theory and Applications*. Addison-Wesley.

- Tikhonov, A.N. and Arsenin, V.Y. (1977). *Solutions of Ill-posed Problems*. Wiley: New York.
- Trujillo, D.M. (1978). "Application of dynamic programming to the general inverse problem". *International Journal for Numerical Methods in Engineering*, 12, 613–624.
- Weaver, W. and Johnston, P.R. (1987). *Structural Dynamics by Finite Elements*. Prentice-Hall, UK.
- Yang, Y.B., Yau, J.D. and Wu, Y.S. (2004). *Vehicle-Bridge Interaction Dynamics*. With Applications to High-Speed Railways, World Scientific Publishing Co., ISBN 981-238-847-8, Singapore.
- Yu, L. and Chan, T.H.T. (2007). "Recent research on identification of moving loads on bridges". *Journal of Sound and Vibration*, 305, 3–21.